HHS Public Access

Author manuscript

J Immunol. Author manuscript; available in PMC 2021 August 02.

Published in final edited form as:

J Immunol. 2020 July 01; 205(1): 143–152. doi:10.4049/jimmunol.1901289.

Placental myeloid cells protect against Zika virus vertical transmission in a Rag1-decifient mouse model

Clayton W. Winkler[*], **Alyssa B. Evans**[*], **Aaron B. Carmody**[†], **Karin E. Peterson**[*,‡]

[*]Laboratory of Persistent Viral Diseases, Rocky Mountain Laboratories, National Institute of Allergy and Infectious Diseases, National Institutes of Health, Hamilton, MT 59840, United States

[†]Research Technologies Branch, Rocky Mountain Laboratories, National Institute of Allergy and Infectious Disease, National Institutes of Health, Hamilton, MT, 59840, United States

Abstract

The ability of Zika virus (ZIKV) to cross the placenta and infect the fetus is a key mechanism by which ZIKV causes microcephaly. How the virus crosses the placenta and the role of the immune response in this process remain unclear. In the current study, we examined how ZIKV infection affected innate immune cells within the placenta and fetus and whether these cells influenced virus vertical transmission (VTx). We found myeloid cells were elevated in the placenta of pregnant ZIKV infected *Rag1*$^{-/-}$ mice treated with an anti-interferon receptor antibody, primarily at the end of pregnancy, as well as transiently in the fetus several days before birth. These cells, which included maternal monocytes/macrophages, neutrophils and fetal myeloid cells contained viral RNA and infectious virus suggesting they may be infected and contributing to viral replication and VTx. However, depletion of monocyte/macrophage myeloid cells from the dam during ZIKV infection resulted in increased ZIKV infection in the fetus. Myeloid cells in the fetus were not depleted in this experiment likely due to an inability of liposome particles containing the cytotoxic drug to cross the placenta. Thus, the increased virus infection in the fetus was not the result of an impaired fetal myeloid response or breakdown of the placental barrier. Collectively, these data suggest that monocyte/macrophage myeloid cells in the placenta play a significant role in inhibiting ZIKV VTx to the fetus, possibly through phagocytosis of virus or virus infected cells.

Introduction

Zika virus (ZIKV) is a flavivirus transmitted primarily by *Aedes* species mosquitoes that is typically asymptomatic or causes only mild febrile disease in humans (1). However, in a 2015 outbreak in Brazil (2), ZIKV was found to be the causative agent contributing to an alarming increase in congenital birth defects (3–5). Most devastating amongst these defects was abnormal fetal nervous system development including calcifications, cortical thinning and aberrant neuronal death associated with virus-induced brain inflammation (6–8). In rarer cases, ZIKV infection in the fetus resulted in microcephaly (9), a severe neurodevelopmental condition characterized by a smaller than average head and brain (10). Implicit in these

[‡]Corresponding Author: Dr. Karin E. Peterson, Rocky Mountain Laboratories, National Institute of Allergy and Infectious Diseases, National Institutes of Health, 903 S. 4th Street, Hamilton, MT 59840. Phone:406-375-9630, Fax:406-375-, petersonka@niaid.nih.gov.

findings is the ability of ZIKV to cross the human placental barrier in viremic mothers to infect the fetus and ultimately the fetal brain. How the virus is transmitted is not fully understood.

Vertical transmission (VTx) of pathogens across the placenta is a rare occurrence, and accounts for only a small percentage of congenital abnormalities (11). This is due to the fact that the placenta is a formidable physical barrier which only a limited number of pathogens can cross (12, 13). This barrier is primarily formed by syncytiotrophoblast cells which are fetal in origin and are generated from fetal cytotrophoblasts that invade, remodel and anchor themselves within uterine decidua to form an intervillous space which is bathed in maternal blood (14). Syncytiotrophoblasts also function to anchor fetal capillaries within the villus space and mediate the exchange of molecules between the two blood supplies. This syncytiotrophoblast layer has been shown to be resistant to infection (11), including by ZIKV, through paracrine type-I interferon (IFN) signaling (15). Thus, ZIKV likely does not cross the placental barrier by directly infecting the syncytiotrophoblast layer but by some other mechanism.

Studies have shown that ZIKV can infect nonsyncytiotrophoblast placental cells (16–18) and induce cellular damage in pregnant mice that is associated with both fetal growth restriction and virus VTx (19, 20). While the cause of this damage remains unclear, ZIKV infection of placental cells can induce the expression of proinflammatory cytokines (21–23) that may both contribute to virus levels as well as mediate placental damage (24, 25). Indeed, a nonhuman primate study demonstrated immune cell infiltration into the placenta in response to ZIKV infection during pregnancy that was correlated with placental dysfunction (26). Additionally, a case report of a ZIKV-infected, spontaneously aborted human pregnancy demonstrated increased amounts of immune cells in the infected placenta (23). Collectively, these data suggest virus-induced immunopathology could be a possible mechanism for ZIKV VTx. Conversely, immune cell infiltration into tissue is not necessarily pathogenic and is commonly required for effective viral control and clearance (27, 28). Thus, a better understanding of what cells are recruited to the placenta and the role those cells have in virus transmission to the fetus is important in determining how to prevent ZIKV-mediated congenital disease.

Of the immune cells that may be involved in ZIKV VTx across the placenta, innate immune cells are of particular interest. Factors involved in the recruitment of innate immune cells are expressed in the ZIKV infected placenta (21–23, 26). Although the role of these cells in the placenta has not been examined, they have been shown to be essential for an effective antiviral response in ZIKV peripheral infection (29, 30). Conversely, they can mediate tissue immunopathology during viral infection (31, 32) which could promote VTx. Innate immune cells may also be relevant to ZIKV VTx in the placenta because both maternal and fetal myeloid cells have been shown to be targets of ZIKV infection (33–35) and could thus play a role in virus replication and trafficking within the placenta.

Several models of ZIKV VTx have been described using IFNAR1$^{-/-}$ mice, hSTAT2 transgenic mice, immunocompetent mice treated with anti-IFNAR antibody and wholly immunocompetent mice (19, 20, 36–39). While useful for pathogenesis studies, these

models either require the use of mouse-adapted virus strains or have confounding factors including maternal weight loss, *in utero* fetal demise or inconsistent VTx. Our previous studies have established that anti-IFNAR1 treatment of pregnant Rag1$^{-/-}$ (AIR) mice results in consistent ZIKV VTx to the fetus following infection with a wildtype Paraiba isolate at 7 days post-conception (40). To our knowledge, this is the only model of wildtype ZIKV VTx without maternal weight loss or high levels of *in utero* fetal demise. Although, AIR mice lack functional T cell responses due to Rag1 deficiency, they still retain a competent type-I interferon (IFN) response as compared to IFNAR1$^{-/-}$ mice which develop pregnancy-confounding disease shortly after infection (19, 41). Thus, the AIR model allows for antibody-mediated antagonism of the type-I IFN response which mimics the anti-IFN effect of ZIKV in human infection (42), making it a useful model to examine the role of innate immune cells in ZIKV VTx. Here we demonstrate that myeloid cells were increased in the placenta following infection and were positive for ZIKV. Surprisingly, these cells did not contribute to vertical transmission, but were instead a key component in reducing the spread of virus to the fetus.

Materials and Methods

Ethics statement

All mouse experiments were approved by Rocky Mountain Laboratories Institutional Animal Care and Use Committee and adhered to the National Institutes of Health guidelines and ethical policies, under protocol# 2018–001E.

Virus

The previously described Paraiba strain of ZIKV (42) was used for all experiments and was kindly provided by Dr. Steven Whitehead (NIH). This strain was isolated from a human clinical case in Paraiba (Brazil) during the outbreak in that country in 2015. Virus working stocks were generated by a single passage of a founder stock in C6/36 cells (ATCC) grown according to the supplier's recommendation with the exception that upon infection, cells were maintained at 30℃. Supernatants were collected at 3 days post infection (dpi) and frozen at 80℃ for future dilution and use. Virus stocks underwent no more than 3 passages.

Generation and infection IgR and AIR mice

Rag1$^{-/-}$ (B6.129S7-*Rag1*^{tm1Mom}/J) mice which are deficient in B and T lymphocytes and mice with global cellular expression of GFP (C57BL/6-Tg(UBC-GFP)30Scha/J) (Jackson Laboratories) were maintained on a C57BL/6 background in a breeding colony at RML. Eight-to-twelve-week-old female *Rag1*$^{-/-}$ mice were treated with anti-IFNAR1 clone MAR1–5A3 to generate AIR (anti-interferon *Rag1*$^{-/-}$) mice or with normal mouse IgG to generate IgR (IgG *Rag1*$^{-/-}$) mice as shown in Fig. 1A and previously described (40). Pregnant mice were inoculated intraperitoneally (i.p.) 5–8 days post mating with 10^4 plaque forming units (PFU) of ZIKV, diluted in sterile 1XPBS, in a volume of 200 μl/mouse. Pregnant, infected IgR and AIR mice were observed daily for signs of neurologic disease or abnormal pregnancy weight gain/loss, however, all mice were clinically unremarkable as previously described (40).

Fetal crosses and experimental usage

Rag1$^{-/-}$ females were bred to congenic *Rag1*$^{-/-}$ males or to global GFP males prior to AIR or IgR treatment to generate crosses for specific experiments (outlined in Fig. 1A). Fetal gender was not determined for these experiments, but entire litters were used for a single analysis.

Placentas and fetuses from *Rag1*$^{-/-}$ x *Rag1*$^{-/-}$ AIR and IgR crosses were used for phenotyping the cellular infiltrate into the placenta and fetus and for VTx studies (Fig. 1, 3, 4, 5A–E, 6 and Sup. Fig. 1, 2–4 and Sup. Fig. 4). For placental phenotyping experiments (Fig. 1B–F), 11-to-36 placentas from each of two-to-four pregnant IgR or AIR mice were analyzed for each time point. For fetal phenotyping experiments (Fig. 5A–E), five-to-ten fetuses from a subset of the pregnancies used in placental phenotyping experiments were analyzed. Eight or more samples were used in the analysis at each time point for each treatment group. Collectively, fifteen AIR pregnancies were used in VTx experiments (Fig. 3, 4, Sup. Fig. 2–4 and Table I) with eight being treated with clodronate and seven treated with control liposomes. Two pregnancies from each treatment were used for depletion verification (Sup. Fig. 2–3). Five clodronate and four control liposomes AIR pregnancies were split between RNA and plaque assay analysis (Fig. 3) and histological analysis (Table I, Fig. 7 D, E). One pregnancy from each treatment was used for an Evans Blue placental leakage experiment (Sup. Fig. 4).

To distinguish maternal and fetal cells for infectious center assay and RNA analysis, *Rag1*$^{-/-}$ females were mated with GFP Tg male mice, so that fetal derived cells were GFP^{+}, while maternal cells were GFP^{-} . These crosses were used for FACs sorting experiments (Fig. 2, 5F, G and Sup. Fig. 1). FACs sorts from placenta (Fig. 2 and Sup. Fig. 1) were performed on pregnancies from four IgR and four AIR dams with two taken on each dpi analyzed (11 and 12dpi). For the fetal sorts (Fig. 5), three IgR and four AIR dams were analyzed, with two of each examined at 11dpi and one IgR and two AIR examined at 12dpi.

Treatment of mice with clodronate or control liposomes

For the depletion of phagocytic myeloid cells, pregnant AIR mice were treated with 125μL i.p. of a 7mg/mL active dose solution of clodronate filled liposomes (Clophosome®, FormuMax) on four days (5, 7, 9 and 11dpi). This every-other-day regiment was adopted as it has been shown to be required for consistent iMO depletion in tissue (43). Controls were given an equivalent volume of control (empty) liposomes on the same schedule. Depletion was validated by flow cytometry (see below).

Flow cytometric phenotyping and validation of depletion of immune cells from placenta and fetus

Placentas and whole fetuses were isolated from pregnant AIR or IgR mice on the indicated days and the tissues were homogenized using a dounce homogenizer, then passed through a 100μm filter to generate a single-cell suspension. At room temperature (rt), RBCs were removed using lysis buffer (0.15 M NH_4Cl, 10 mM $KHCO_3$, 0.1 M EDTA), and cells were washed with 0.4% BSA in 1xPBS and passed through a 70μm filter to remove cellular debris. Cells were then surface stained with primary-conjugate antibodies for 30–45 min at

4°C in the dark. The antibodies used for cell staining were purchased from BD Pharmingen, eBioscience, or BioLegend, unless otherwise noted. The following antibody combination was used: CD86–PE, F480–APC, CD11b-Brilliant Violet 510, CD45-APC/Cy7, Ly6C-AF700, Ly6G-Pacific Blue and CD11c-PE/Cy7. Cells were fixed in 4% paraformaldehyde in 1xPBS, washed with 1xPBS and data were acquired on a FACSymphony A5 cytometer (BD Biosciences). Gates were used to exclude cellular debris and doublets (Fig.1 A, E) and the $CD45^+$, $CD11b^+$ myeloid population identified (Fig.1 B, F). $Ly6G^+$ neutrophils (granulocytes) and $Ly6C^+$ monocytes (iMOs) were identified within the $CD45^+$, $CD11b^+$ gate (Fig. 1 C, G) and the remaining macrophage/other myeloid population were assayed for F4/80 and CD86 expression (Fig. 1 D, H). An abbreviated version of this gating is shown in Fig. 3 for the clodronate depletion experiments with the alteration that macrophages and other myeloid cells are grouped together. Each of the identified populations were examined for CD11c expression and found to be negative (not shown). All analysis was performed using FCS Express v5 software (DeNovo Software).

FACs sorting of immune cells from placenta and fetus

Placental and fetal single cell suspensions were generated as described above from placentas and fetuses from *Rag1*$^{-/-}$ female x GFP^+ male matings. Cells were then run through a 0-30-70% Percoll gradient as previously described (44) and collected at the 70–30% interface to concentrate the immune cell population. Cells were then washed with 2%BSA in 1xPBS and surfaced stained as described above. The following antibody combination was used: CD11b-APC, CD45-PE, Ly6C-AF700 and Ly6G-PB. Cells were then sort on a four channel FACsAria IIu (BD Biosciences). Cells from placenta or fetus were first sorted based on their GFP expression to distinguish maternal from fetal cells. Next, in the placenta, $CD45^+$ $CD11b^+$ fetal myeloid cells were sorted and collected as a bulk population. Conversely in the fetus, CD45+ CD11b+ maternal myeloid cells were sorted and collected. Then, remaining unsorted maternal or fetal cells populations from placenta or fetus respectively were then sorted by Ly6G and Ly6C expression to identify neutrophils and monocytes (iMOs) respectively and collected. Finally, the remaining $Ly6G^-$ and $Ly6C^{low}$ populations from each were collected as the final bulk myeloid population. A graphic of this gating strategy for placenta in shown in Sup. Fig. 2. The same strategy was used for fetal tissue except that maternal myeloid cells were collected as a bulk population (Sup. Fig. 1I–M) and fetal myeloid cells were sorted based on Ly6G and Ly6C expression as described above (Sup. Fig. 1L–P). Sorts contained between ~1500–50,000 cells dependent on the cell type and tissue being sorted. Cells were sorted into either ZR RNA buffer (Zymo Research) and immediately processed for RNA isolation or into DMEM cell medium culture containing 2% fetal bovine serum for infectious center assay.

Infectious center assay

Sorted myeloid cells population (see above) were plated onto confluent Vero cells in 24 well plates at a known number of cells (events) per well. Immediately following plating, 500 μl of 1.5% carboxymethyl cellulose in MEM was overlaid onto the cells, and the cells were incubated undisturbed at 37°C for 5 d. Then cells were fixed by adding 10% formaldehyde to each well until full and allowed to sit for 1 h at rt. After fixation, plates were rinsed gently with deionized water and stained with 0.35% Crystal violet for 15 min. Plates were rinsed

and allowed to air dry in an inverted position. The number of infectious centers per well was determined by plaque counts. Data is presented as number of plaques per 1000 cells (events) plated into each well.

Real-time quantitative PCR

Real-time PCR analysis of mRNA expression from FACs sorted cells, placenta, fetal body or fetal brain was completed as previously described (45). The primers used included Gapdh.2–152F (5′-TGCACCACCAACTGCTTAGC-3′), Gapdh.2–342R (5′-TGGATGCAGGGATGATGTTC-3′), ZIKVFP8008F (5′-AAGCTGAGATGGTTGGTGGA-3′), and ZIKVFP8121R (5′-TTGAACTTTGCGGATGGTGG-3′). Primers were subjected to BLAST analysis (National Center for Biotechnology Information) to ensure detection of only the specified gene and were tested on positive controls to ensure amplification of a single product. Data for each sample were calculated as the percentage difference in threshold cycle (C_T) value ($\Delta C_T = C_T$ for GAPDH gene $- C_T$ for specified gene). Gene expression was plotted as the percentage of gene expression relative to that of the GAPDH gene.

Plaque assays for ZIKV in tissues

Placenta and fetal bodies and brains from ZIKV-infected mice were weighed and placed in 2ml tubes with 2.3mm zirconia/silica beads (BioSpec). Serum-free DMEM was added to the tubes at volumes of 500μl for placentas, 250μl for fetal brains, and 750μl for fetal bodies. Samples were then homogenized on a Bead Mill 24 (Fisher) at 5300 rpm for 25 seconds. Homogenates were clarified at 5000xg for 10 minutes at 4C, and the supernatant was transferred to new tubes. Fetal bodies were clarified a second time. Serially diluted solution from clarified samples was added to confluent Vero cells in a 24-well plate and incubated again for 1 h at 37°C. After incubation, plates were treated the same as described in the infectious center assay above. Viral titer was calculated by dividing the number of plaques per given sample by the mg plated per well, based on starting tissue weight/volume. Data are reported as PFU per mg of tissue

Immunohistochemistry and in situ hybridization

At the experimental end point, some placentas and fetuses (Table I) were bisected along the dorsal midline to expose internal organs and placed in 10% neutral buffered formalin. Whole tissues were serially sectioned (5 μm) and mounted on slides. For immunohistochemistry, sections were blocked (5% BSA, 0.05% Triton in PBS) at rt for 1 h and then primary antibodies against ZIKV NS5 (1:3000; Aves Labs) and ionized calcium binding adaptor protein 1 (Iba1, 1:250; Dako) were applied and incubated overnight at 4°C in blocking buffer. Secondary antibodies were used to label specific primaries (goat anti-chicken Alexa Fluor 488 and donkey anti-rabbit Alexa Fluor 594). Secondaries were incubated for 1 h at rt. Hoechst (ThermoFischer) was used to label cell nuclei according to the manufacturer's instructions. Number 1.5 coverslips were applied over ProLong Gold mounting medium I (nuclei, Molecular Probes) prior to imaging. All slides were then imaged using a Zeiss Axio Scan.Z1 (Carl Zeiss) with a Plan-Apochromat 40x objective (NA 0.95) make composite images (Fig. 5 and Sup Fig. 1).

Evans Blue injection of infected pregnant AIR mice

To examine vascular leak across the placenta during ZIKV infection, Evans Blue dye was administered intravenously to pregnant AIR mice at 11dpi as previously describedhttps://www.nature.com/articles/s41598-017-07099-7-ref-CR25 (46). Following injection, whole fetuses were dissected and fixed with 10% neutral buffered formalin. Whole pups were imaged with an Olympus SZX16 dissection scope coupled to an Olympus DP25 camera.

Statistical analysis

All statistical analyses were performed using Prism 7.01 software (GraphPad). The statistical test for each experiment is described in the figure legends.

Results

Myeloid cell proportions are elevated in the placenta of ZIKV infected AIR mice late in pregnancy

ZIKV can infect the placenta (6, 40) causing inflammation (23, 26). However, the makeup of this inflammatory response or how it influences viral VTx is not well understood. We used ZIKV-infected, pregnant anti-interferon antibody treated, *Rag1*$^{-/-}$ (AIR) mice (40) to study the myeloid cellular immune response in the placenta over time (Fig. 1A, blue). In this model, dams were treated with anti-IFNAR1 antibody at −1, 3, 7 and 11 days post inoculation (dpi) starting at 5–7 days of pregnancy and infected with ZIKV at 6–8 days of pregnancy. Time point matched IgG treated *Rag1*$^{-/-}$ (IgR) mice were used as experimental controls as these mice are genotypically identical, but control virus infection sufficiently to prevent infection of the placenta and VTx to the fetus (40). Flow cytometric analysis of placenta samples from ZIKV infected AIR mice showed a proportional increase in CD45^{+} CD11b^{+} myeloid cells compared to IgR controls beginning at 7 days post infection (dpi) corresponding to embryonic day (E)11–14 (Sup. Fig. 1 B, F and Fig. 1 B). This infiltration peaked at 11dpi (E15–18) and was sustained through 12dpi, just prior to birth (~E16–19).

To better understand the type of myeloid cells infiltrating the placenta, markers for specific cell types were analyzed and reported as a proportion of the entire placenta. Ly6G^{+} neutrophils were increased in placentas of AIR mice compared to IgR mice at 7 (E11–14), 11 (E15–18) and 12dpi (E16–19) (Sup. Fig. 1C, G and Fig. 1C). Ly6C^{+} inflammatory monocytes (iMOs) were proportionally higher in AIR mice placenta from 10dpi through the end of the experiment (Sup. Fig. 1C, G and Fig. 1D). The Ly6C^{low} Ly6G^{-} population of CD45^{+} CD11b^{+} myeloid cells in the placenta contained F480^{+} macrophages, F480^{+} CD86^{+} double positive macrophages (populations shown in Sup Fig. 1. D, H). Analysis of this cell population showed increased proportions of both F480^{+} and F480^{+} CD86^{+} double positive macrophages in AIR placentas later in pregnancy relative to IgR controls, with the largest differences being at 11dpi, but continuing through to near birth at 12dpi (Fig. 1E, F). These findings demonstrate an increase of myeloid cell types, including monocytes, neutrophils and other myeloid cells, in the placenta at later stages of pregnancy during ZIKV infection. This increase of myeloid cells could influence transmission of virus to the fetus as well as fetal development.

Myeloid cells in the placenta contain ZIKV RNA and infectious virus

The function of myeloid cells in the ZIKV infected placenta is unclear. These cells may be involved in viral clearance or alternatively be infected by the virus and contribute to virus replication or both at once. To examine these possibilities, myeloid cells in the placenta were isolated by fluorescent activated cell sorting (FACs) from ZIKV infected AIR and IgR mice at 11 and 12dpi (E15–18 and E16–19 respectively) and assayed for infectious virus (11dpi) or viral RNA (12dpi) (Fig. 1A, green). Because placental myeloid cells can be of either maternal or fetal origin, AIR or IgR female mice were bred with male mice globally expressing GFP to generate heterozygous GFP^+ fetuses. Thus, maternal myeloid cells were GFP^-, while fetal myeloid cells were GFP^+ and easily distinguishable (Sup. Fig. 1I, M). From both IgR and AIR placentas, $CD45^+$ $CD11b^+$ fetal myeloid cells were identified and collected (Sup. Fig. 1J, N). Additionally, $CD45^+$ $CD11b^+$ maternal myeloid cells were gated on (Sup. Fig. 1K, O) and sorted by $Ly6G^+$ and $Ly6C^+$ expression to discriminate neutrophils and monocytes as described above (Sup. Fig. 1L, P). The remaining $Ly6G^-$ and $Ly6C^{low}$ myeloid population was also collected as a general maternal myeloid population. This protocol resulted in a total of four sorted populations: 1) $Ly6C^+$ maternal iMOs, 2) $Ly6G^+$ maternal neutrophils, 3) $CD45^+$ $CD11b^+$ $Ly6G^-$ $Ly6C^-$ maternal myeloid cells, and 4) $CD45^+$ $CD11b^+$ $Ly6G^-$ $Ly6C^-$ GFP^+ fetal myeloid cells. Infectious center assays (Fig. 2A) or quantitative reverse-transcription PCR (qRT-PCR) analysis of ZIKV RNA (Fig. 2B) was performed on each of the four isolated myeloid populations from infected IgR and AIR mice at 11 and 12 dpi respectively. All four populations of cells, including fetal myeloid cells, from the placentas of AIR mice were positive for both infectious ZIKV and ZIKV RNA, while cells from IgR mice were generally below the level of detection. Thus, during late-stage pregnancy in ZIKV infected AIR mice, both maternal and fetal placenta myeloid cells appear to be infected suggesting they could be contributing to virus production. However, it remains unclear what role these cells play in ZIKV VTx.

Depletion of myeloid cells in placenta by clodronate liposomes

To examine a roll for myeloid cells in ZIKV VTx across the placenta, clodronate was used to deplete phagocytic myeloid cells in pregnant, ZIKV-infected AIR mice (Fig. 1A, red). To validate effective depletion, 12dpi placentas from infected AIR mice treated with either control empty liposomes (Sup. Fig. 2A) or clodronate containing liposomes (Sup. Fig. 2B) were analyzed by flow cytometry. The overall proportion of $CD45^+CD11b^+$ positive myeloid cells was significantly reduced in clodronate treated animals (Sup. Fig. 2A–C). Analysis of separate cell types showed that clodronate treatment did not alter the proportions of neutrophils but did significantly reduce the proportions of other remaining myeloid cell population including both maternal and fetal macrophages but also $Ly6C^+$ iMOs (Sup. Fig. 2C). Thus, clodronate treatment effectively depleted inflammatory monocytes and other non-neutrophil myeloid cells from the placenta of ZIKV infected AIR mice.

Myeloid cell depletion increases VTx to the fetus.

From previous work, VTx of ZIKV to the fetus occurs primarily between 10–12dpi in the AIR model (40) (data not shown). Therefore, because myeloid cells peaked in the placenta at 11–12dpi (Fig. 1B), we examined individual placentas, fetal bodies and fetal brains from

ZIKV-infected AIR mice treated with control or clodronate liposomes at these time points for viral RNA (Fig. 3A–C) and infectious virus by plaque assay (Fig. 3D–F). Placentas from clodronate treated AIR mice contained similar amounts of viral RNA and infectious virus compared to day-matched controls at both time points examined, indicating myeloid cell depletion did not significantly alter viral infection in this organ (Fig. 3A, D).

At 11dpi, viral RNA and infectious virus levels were similar in the fetal body of control and clodronate treated samples (Fig. 3B, E). However, one day later, a significant increase in viral RNA and infectious virus was observed in fetuses from the clodronate-treated group (Fig. 3B, E). Increased viral RNA and infectious virus was also found in the fetal brain of clodronate treated samples at 12dpi (Fig. 3C, F) relative to controls. These data suggest myeloid cells recruited to the placenta during ZIKV infection actively inhibit viral VTx at a critical time point late in pregnancy.

ZIKV infection is wide spread in fetuses from clodronate treated dams

To compare the extent of viral infection within fetuses from dams treated with clodronate relative to dams treated with control liposome, whole-mount immunohistochemistry was performed on samples at 12dpi (Fig. 4 and Table I). For each fetus, two bilateral sections taken ~1mm off the midline were labeled for ZIKV antigen and Iba1 and analyzed. ZIKV antigen was detectable somewhere within the entire fetus in ~39% of samples from control liposome treated AIR dams but in ~81% of clodronate treated samples (Table I) confirming increased ZIKV VTx. In positive samples from both groups, viral antigen was consistently found in the lymphatics, the nasal turbinates (Fig. 4A, B and e, i) and in the soft tissues of the neck in and around the submaxillary salivary gland (Fig. 4A, B and f, j). However, clodronate treated samples typically had more widespread viral antigen throughout the body (Fig. 4B, Table I, white signal) compared to control treated samples (Fig 4A, Table I). Two litters in particular, XZ316–1 and XZ316–2, had pups with widespread infection throughout the whole body (Table I). These were litters with the most pronounced visual decrease in myeloid cell-specific ionized calcium binding adaptor 1 (Iba1) labeling in the placenta (Sup. Fig. 2D vs. E, magenta signal in insets), particularly in the maternal decidual space (area above the yellow line) indicating they had the largest decrease in phagocytic myeloid cells. Thus, myeloid cells recruited to the placenta during ZIKV infection seem to protect against, rather than contribute to, VTx of ZIKV to the fetus.

Protection against VTx of ZIKV occurs in placenta not fetus.

Myeloid cells might also suppress fetal infection by antiviral actions within the fetus. Therefore, we analyzed myeloid cells from some of the fetuses of the same pregnancy experiments described in Fig. 1 via the same methods. AIR fetuses had proportionally more fetal myeloid cells overall compared to IgR controls at 11 dpi (Fig. 4A–E). This increase was also found in the fetal neutrophil, and fetal iMO populations. However, these differences resolved by 12 dpi indicating that this increase was a short-lived response. GFP^+ FACs sorting of myeloid cells from the same infected AIR fetuses shown in Fig. 2, demonstrated little to no detectable infectious virus in any myeloid cell group (Fig. 5F) at 11dpi. One day later fetal iMOs consistently contained detectable levels of viral RNA, suggesting they were either infected or attempting to clear virus (Fig. 5G). These cells may be analogous to the

Iba1 and ZIKV NS5 dual positive cells observed in control liposome treated fetuses from infected AIR mice (Fig. 4 f, yellow arrow). However, neutrophils and other fetal myeloid cells isolated by FACs from infected AIR fetuses rarely contained detectable viral RNA, suggesting they played little role in either viral replication or clearance. On 12dpi, maternal myeloid cells (GFP^-) were collected so infrequently that they are unlikely to play a significant role in protecting the fetus from ZIKV infection. Furthermore, analysis of the same clodronate liposome treated mice from the experiments outlined in Figs. 3 and 4 showed no reduction of fetal cells (Sup. Fig. 3A), indicating that the increase in virus in the fetus following clodronate treatment was not due to a reduction in myeloid cells in the fetus. This was confirmed by immohistochemical labeling of umbilical cord from fetuses in Table I (Sup. Fig. 3B, C), which consistently showed $Iba1^+$ cells present in both conditions. Thus, the effect of myeloid cells on controlling ZIKV infection in the fetus appears to be due to placental myeloid cells, rather than fetal myeloid cells.

Our data to this point suggests that myeloid cells in the placenta function to clear ZIKV (Fig. 2), thus inhibiting VTx (Fig. 3). However, an alternative hypothesis could be that myeloid cells in the placenta function to maintain the placental barrier during ZIKV infection to prevent VTx. To test this, we administered Evans Blue dye to ZIKV infected AIR dams treated with clodronate or control liposomes and visually examined the fetuses for dye leakage into the umbilical cord or body of the animal (Sup. Fig. 4A, B). Despite there being a vivid blue dye coloring in the placentas of clodronate treated animals, there was no observable dye leakage into the umbilical cord or the body of the animal in either treatment group. Therefore, we concluded that monocyte/macrophages do not play a significant role in maintenance of the placental barrier.

Discussion

ZIKV is a human pathogen of concern that can be vertically transmitted (VTx) to an unborn fetus. It is possible that innate immune cells could play a role in ZIKV VTx and pathogenesis (33, 47). Therefore, in this study we examined the innate cellular inflammatory response in the placenta following ZIKV infection. We found an influx of myeloid cells in response to ZIKV infection, including infected myeloid cells. However, treatment of pregnant ZIKV infected mice with clodronate containing liposomes resulted in enhanced virus levels in the fetus (Fig. 3). The primary cells depleted in the placenta by clodronate were monocyte/macrophages (Sup. Fig. 2). These were also the cells that were the most consistently elevated in the placenta during ZIKV infection (Fig. 1) at the time of VTx (Fig 3B, C and unpublished observations), suggesting they are critical to the antiviral response in this tissue.

Previous studies have shown that myeloid cells, in particular monocyte/macrophages and Hofbauer cells, are susceptible to ZIKV infection (18, 33). However, it was unknown whether these cells contribute to viral replication in the ZIKV infected placenta. Our data showed that both maternal and fetal myeloid cells in the placenta contained some infectious virus and viral RNA (Fig. 2). These findings suggest placental myeloid cells could be infected with ZIKV or actively phagocytosing virus and virus infected cells to aid in viral clearance or both simultaneously. However, viral RNA in the placenta did not significantly

change when myeloid cells were depleted with clodronate (Fig. 3A), suggesting these cells are not primary sites of viral replication. Furthermore, myeloid cell depletion resulted in a significant increase in ZIKV VTx at the critical 12dpi time point indicating these cells primarily function as a barrier to VTx (Fig. 3B, C). Thus, other placental cells may be responsible for the high levels of virus in the placenta. These might include maternal decidual cells, amniotic epithelial cells, fetal cytotrophoblasts and trophoblast progenitors which have been shown to express known viral entry receptors (16, 17). Also, villous fibroblasts have been shown to be susceptible in placental explants (18).

We found that both maternal and fetal myeloid cells in the placenta of AIR, but not IgR mice were infected with ZIKV (Fig. 2). This is consistent with previous findings which indicate myeloid cells are susceptible to ZIKV infection (33–35). However, myeloid cells in the placenta of AIR mice were minimally infected at 11dpi because, at most, only ~4 infectious centers per 1000 cells was observed in any myeloid cell type (Fig. 2A). Viral RNA was 2–3 logs higher in myeloid cells in AIR vs IgR mice one day later in the placenta (Fig. 2B). However, this difference could be accounted for by the phagocytic function of myeloid cells, which may phagocytose and kill viruses or viral debris rather than being directly infected. Consistent with this idea, infectious virus titers increased slightly in the placenta as a whole at 11 and 12 dpi when myeloid cells were depleted suggesting that the role of monocyte/macrophages results in a net decrease in infectious virus (Fig. 3D). This has also been demonstrated for other pathogens that can infect the placenta (48). However, the exact mechanism by which myeloid cells control ZIKV remains unclear. ZIKV infection can shift peripheral monocyte/macrophage activation toward a more anti-inflammatory phenotype, which is generally more conducive to viral replication and dissemination (34, 49). We found a similar result, where the majority of $CD45^+$, $CD11b^+$, $F480^+$ macrophages from the placenta of ZIKV infected AIR mice were negative for the activation marker CD86 (Fig. 1E), which is more consistent with an anti-inflammatory phenotype in mice (50). It may be that in the placenta, anti-inflammatory macrophages have a more robust antiviral effect than in the periphery, although additional experimentation is required. Indeed, pregnancy-associated anti-inflammatory macrophages have high phagocytic activity (51, 52). Thus, enhancing the effect of placental anti-inflammatory macrophages during ZIKV pregnancy may result in more positive outcomes.

Our findings indicate that myeloid cells likely inhibit ZIKV VTx likely through an antiviral mechanism. However, we also investigated the possibility that myeloid cells could be preventing VTx by stabilizing the placental barrier (Sup. Fig. 4). We did this by injecting Evans Blue dye into ZIKV-infected control or clodronate treated pregnant AIR mice and examined the resulting fetuses for dye leakage. Evans Blue directly binds to albumin in the maternal blood, but albumin does not cross the placental barrier during normal pregnancy (53). Therefore, leakage of dye into the umbilical cord or fetus would be an indication of large-scale breakdown of the placental barrier. This experimental approach was somewhat limited in that small amounts of Evans Blue dye leakage could have been below the limits of detection by this assay. However, the clodronate drug itself was not able to cross the placental barrier and deplete myeloid cells in the fetus, even at the time of ZIKV VTx (Sup. Fig. 3). Clodronate liposomes range in size, but standard preparations (54) have particles that overlap in size with the diameter of ZIKV (55). Therefore, both Evans Blue dye and the

lack of myeloid cell depletion in the fetus indicate that the placental barrier likely remains intact during ZIKV infection even during late-stage pregnancy.

In addition to myeloid cells, we did observe an increase in $Ly6G^+$ neutrophils in the placenta at 11–12 dpi of ZIKV-infected pregnant mice compared to uninfected controls (Fig. 1J) and these cells were positive for ZIKV RNA (Fig 2B). Neutrophils are known to produce important antiviral factors such as cytokines and reactive oxygen species and to release extracellular traps that capture and eliminate virions (56). However, these factors must be tightly controlled otherwise they can lead to tissue damage (57). Consistent with this idea, we observed that the proportion of neutrophils in the placenta fluctuated throughout disease suggesting they may be modulated to minimize their pathogenic effect (Fig. 1J). Furthermore, we could not determine a role for neutrophils in this study as these cells were not depleted by clodronate (58). Thus, we did not focus on this population in these studies. Further studies depleting these cells may indicate whether this transient population has a positive or negative effect on ZIKV transmission to the fetus.

Here we examined myeloid responses to ZIKV infection in the placenta and fetus using a human isolate WT strain of ZIKV. This is advantageous to a recently published model using mouse-adapted ZIKV because the effect of the WT virus on the innate immune response is unaltered. Generation of mouse-adapted virus involved the iterative passage of WT ZIKV through the same *Rag1*$^{-/-}$ mice used here resulting in a virus with three nonsynonymous mutations that enhanced virus infection in mice (36). While the effects of these virus mutations on the immune response in mice have not yet been investigated, because *Rag1*$^{-/-}$ mice retain a functional innate response, the mutations are likely adaptations for evasion of the innate immune response. Thus, interpreting myeloid cell responses to mouse adapted ZIKV would be challenging. Furthermore, because even single nucleotide polymorphisms can drastically alter susceptibility in mice to ZIKV (59) and also likely their immune response, we focused on WT virus for these studies.

One of the cell types not analyzed in this study were T cells. We could not examine the role of these cells in ZIKV VTx in our model because we are utilizing $Rag1^{-/-}$ mice. It is necessary for us to use these mice because the absence of T- and B- cells along with the application of an anti-interferon antibody is required to generate sufficient viral titers to develop consistent VTx (45, 47). Attempts to examine ZIKV VTx in WT mice have resulted in intrauterine growth restriction (19), inconsistent or no transmission (20, 38) or required the use mouse adapted ZIKV strains (36, 39). The alternative would be to attempt these studies in ZIKV infected, pregnant $IFNAR1^{-/-}$ mice which have impaired innate immune responses, including impaired monocyte/macrophage recruitment to sites of viral infection (31) and have confounded variables during pregnancy including maternal death, weight loss and fetal insufficiency (19, 38). Instead, we took advantage of the AIR model, where we only transiently blocking the interferon response with an antibody which allows for establishment of viral infection but does not completely block innate immune responses or cellular recruitment (Fig. 1). Furthermore, we selected an inoculation time point for these studies that correlated with late first trimester, early second trimester in human pregnancy when teratogenic ZIKV VTx has been reported (7, 60). Collectively this approach allowed

us to examine the role of the cellular innate immune response in a murine model that closely resembles the effects of ZIKV infection at a critical time point during pregnancy.

Previous studies have shown cytotoxic T cells are elevated in the placenta during ZIKV infection in primates and humans (23, 26). Furthermore, we found increased granzyme B+ CD8+ T cell responses to ZIKV infection in wildtype mice and showed that depletion of CD8 and CD4 T cells resulted in increased disease in WT mice (45). However, pregnancy dramatically decreased $CD8^+$ T cell responses to ZIKV, with a significant reduction in Ki67, CD11a+ CD43+ and GranzB+ T cells to near basal levels (45). Nevertheless, further studies regarding whether these CD8+ T cells have a role in ZIKV transmission and whether CD8+ T cells are influenced by the anti-inflammatory M2-like cells identified in this study would further clarify how immune cells in the placenta regulate vertical transmission of ZIKV.

Supplementary Material

Refer to Web version on PubMed Central for supplementary material.

Acknowledgements

The authors thank Dr. Lara Meyers, Dr. Olof Nilsson and Dr. Natalia Malachowa for critical reading of the manuscript, Dan Long and Nancy Kurtz for processing and sectioning tissues and Anita Mora and Ryan Kissinger for assistance with illustrations. We also thank Jeff Severson and Shelby Malingo for outstanding animal husbandry with pregnant animals.

Financial disclosure: This work was supported by the Division of Intramural Research, National Institute of Allergy and Infectious Disease (AI001102–11)

References

1. Campos GS, Bandeira AC, and Sardi SI. 2015. Zika Virus Outbreak, Bahia, Brazil. Emerg Infect Dis 21: 1885–1886. [PubMed: 26401719]
2. Zanluca C, Melo VC, Mosimann AL, Santos GI, Santos CN, and Luz K. 2015. First report of autochthonous transmission of Zika virus in Brazil. Mem Inst Oswaldo Cruz 110: 569–572. [PubMed: 26061233]
3. Tang BL 2016. Zika virus as a causative agent for primary microencephaly: the evidence so far. Arch Microbiol 198: 595–601. [PubMed: 27412681]
4. Brasil P, Pereira JP Jr., Moreira ME, Ribeiro Nogueira RM, Damasceno L, Wakimoto M, Rabello RS, Valderramos SG, Halai UA, Salles TS, Zin AA, Horovitz D, Daltro P, Boechat M, Raja Gabaglia C, Carvalho de Sequeira P, Pilotto JH, Medialdea-Carrera R, Cotrim da Cunha D, Abreu de Carvalho LM, Pone M, Machado Siqueira A, Calvet GA, Rodrigues Baiao AE, Neves ES, Nassar de Carvalho PR, Hasue RH, Marschik PB, Einspieler C, Janzen C, Cherry JD, Bispo de Filippis AM, and Nielsen-Saines K. 2016. Zika Virus Infection in Pregnant Women in Rio de Janeiro. N Engl J Med 375: 2321–2334. [PubMed: 26943629]
5. Barcellos C, Xavier DR, Pavao AL, Boccolini CS, Pina MF, Pedroso M, Romero D, and Romao AR. 2016. Increased Hospitalizations for Neuropathies as Indicators of Zika Virus Infection, according to Health Information System Data, Brazil. Emerg Infect Dis 22: 1894–1899. [PubMed: 27603576]
6. Driggers RW, Ho CY, Korhonen EM, Kuivanen S, Jaaskelainen AJ, Smura T, Rosenberg A, Hill DA, DeBiasi RL, Vezina G, Timofeev J, Rodriguez FJ, Levanov L, Razak J, Iyengar P, Hennenfent A, Kennedy R, Lanciotti R, du Plessis A, and Vapalahti O. 2016. Zika Virus Infection with Prolonged Maternal Viremia and Fetal Brain Abnormalities. N Engl J Med 374: 2142–2151. [PubMed: 27028667]

7. Mlakar J, Korva M, Tul N, Popovic M, Poljsak-Prijatelj M, Mraz J, Kolenc M, Resman Rus K, Vesnaver Vipotnik T, Fabjan Vodusek V, Vizjak A, Pizem J, Petrovec M, and Avsic Zupanc T. 2016. Zika Virus Associated with Microcephaly. N Engl J Med 374: 951–958. [PubMed: 26862926]
8. Moore CA, Staples JE, Dobyns WB, Pessoa A, Ventura CV, Fonseca EB, Ribeiro EM, Ventura LO, Neto NN, Arena JF, and Rasmussen SA. 2017. Characterizing the Pattern of Anomalies in Congenital Zika Syndrome for Pediatric Clinicians. JAMA Pediatr 171: 288–295. [PubMed: 27812690]
9. de Araujo TVB, Ximenes RAA, Miranda-Filho DB, Souza WV, Montarroyos UR, de Melo APL, Valongueiro S, de Albuquerque M, Braga C, Filho SPB, Cordeiro MT, Vazquez E, Cruz D, Henriques CMP, Bezerra LCA, Castanha P, Dhalia R, Marques-Junior ETA, Martelli CMT, Rodrigues LC, G. investigators from the Microcephaly Epidemic Research, H. Brazilian Ministry of, O. Pan American Health, F. Instituto de Medicina Integral Professor Fernando, and P. State Health Department of. 2018. Association between microcephaly, Zika virus infection, and other risk factors in Brazil: final report of a case-control study. Lancet Infect Dis 18: 328–336. [PubMed: 29242091]
10. Hanzlik E, and Gigante J. 2017. Microcephaly. Children (Basel) 4.
11. Arora N, Sadovsky Y, Dermody TS, and Coyne CB. 2017. Microbial Vertical Transmission during Human Pregnancy. Cell Host Microbe 21: 561–567. [PubMed: 28494237]
12. Robbins JR, and Bakardjiev AI. 2012. Pathogens and the placental fortress. Curr Opin Microbiol 15: 36–43. [PubMed: 22169833]
13. Delorme-Axford E, Sadovsky Y, and Coyne CB. 2014. The Placenta as a Barrier to Viral Infections. Annu Rev Virol 1: 133–146. [PubMed: 26958718]
14. Maltepe E, Bakardjiev AI, and Fisher SJ. 2010. The placenta: transcriptional, epigenetic, and physiological integration during development. J Clin Invest 120: 1016–1025. [PubMed: 20364099]
15. Bayer A, Lennemann NJ, Ouyang Y, Bramley JC, Morosky S, Marques ET Jr., Cherry S, Sadovsky Y, and Coyne CB. 2016. Type III Interferons Produced by Human Placental Trophoblasts Confer Protection against Zika Virus Infection. Cell Host Microbe 19: 705–712. [PubMed: 27066743]
16. Tabata T, Petitt M, Puerta-Guardo H, Michlmayr D, Wang C, Fang-Hoover J, Harris E, and Pereira L. 2016. Zika Virus Targets Different Primary Human Placental Cells, Suggesting Two Routes for Vertical Transmission. Cell Host Microbe 20: 155–166. [PubMed: 27443522]
17. Quicke KM, Bowen JR, Johnson EL, McDonald CE, Ma H, O'Neal JT, Rajakumar A, Wrammert J, Rimawi BH, Pulendran B, Schinazi RF, Chakraborty R, and Suthar MS. 2016. Zika Virus Infects Human Placental Macrophages. Cell Host Microbe 20: 83–90. [PubMed: 27247001]
18. Jurado KA, Simoni MK, Tang Z, Uraki R, Hwang J, Householder S, Wu M, Lindenbach BD, Abrahams VM, Guller S, and Fikrig E. 2016. Zika virus productively infects primary human placenta-specific macrophages. JCI Insight 1.
19. Miner JJ, Cao B, Govero J, Smith AM, Fernandez E, Cabrera OH, Garber C, Noll M, Klein RS, Noguchi KK, Mysorekar IU, and Diamond MS. 2016. Zika Virus Infection during Pregnancy in Mice Causes Placental Damage and Fetal Demise. Cell 165: 1081–1091. [PubMed: 27180225]
20. Szaba FM, Tighe M, Kummer LW, Lanzer KG, Ward JM, Lanthier P, Kim IJ, Kuki A, Blackman MA, Thomas SJ, and Lin JS. 2018. Zika virus infection in immunocompetent pregnant mice causes fetal damage and placental pathology in the absence of fetal infection. PLoS Pathog 14: e1006994. [PubMed: 29634758]
21. Luo H, Winkelmann ER, Fernandez-Salas I, Li L, Mayer SV, Danis-Lozano R, Sanchez-Casas RM, Vasilakis N, Tesh R, Barrett AD, Weaver SC, and Wang T. 2018. Zika, dengue and yellow fever viruses induce differential anti-viral immune responses in human monocytic and first trimester trophoblast cells. Antiviral Res 151: 55–62. [PubMed: 29331320]
22. Lei J, Vermillion MS, Jia B, Xie H, Xie L, McLane MW, Sheffield JS, Pekosz A, Brown A, Klein SL, and Burd I. 2019. IL-1 receptor antagonist therapy mitigates placental dysfunction and perinatal injury following Zika virus infection. JCI Insight 4.
23. Rabelo K, Souza LJ, Salomao NG, Oliveira ERA, Sentinelli LP, Lacerda MS, Saraquino PB, Rosman FC, Basilio-de-Oliveira R, Carvalho JJ, and Paes MV. 2018. Placental Inflammation and Fetal Injury in a Rare Zika Case Associated With Guillain-Barre Syndrome and Abortion. Front Microbiol 9: 1018. [PubMed: 29867903]

24. Hurtado CW, Golden-Mason L, Brocato M, Krull M, Narkewicz MR, and Rosen HR. 2010. Innate immune function in placenta and cord blood of hepatitis C--seropositive mother-infant dyads. PLoS One 5: e12232. [PubMed: 20814429]
25. Leon-Juarez M, Martinez-Castillo M, Gonzalez-Garcia LD, Helguera-Repetto AC, Zaga-Clavellina V, Garcia-Cordero J, Flores-Pliego A, Herrera-Salazar A, Vazquez-Martinez ER, and Reyes-Munoz E. 2017. Cellular and molecular mechanisms of viral infection in the human placenta. Pathog Dis 75.
26. Hirsch AJ, Roberts VHJ, Grigsby PL, Haese N, Schabel MC, Wang X, Lo JO, Liu Z, Kroenke CD, Smith JL, Kelleher M, Broeckel R, Kreklywich CN, Parkins CJ, Denton M, Smith P, DeFilippis V, Messer W, Nelson JA, Hennebold JD, Grafe M, Colgin L, Lewis A, Ducore R, Swanson T, Legasse AW, Axthelm MK, MacAllister R, Moses AV, Morgan TK, Frias AE, and Streblow DN. 2018. Zika virus infection in pregnant rhesus macaques causes placental dysfunction and immunopathology. Nat Commun 9: 263. [PubMed: 29343712]
27. Erlebacher A 2013. Immunology of the maternal-fetal interface. Annu Rev Immunol 31: 387–411. [PubMed: 23298207]
28. Racicot K, and Mor G. 2017. Risks associated with viral infections during pregnancy. J Clin Invest 127: 1591–1599. [PubMed: 28459427]
29. Stegelmeier AA, van Vloten JP, Mould RC, Klafuric EM, Minott JA, Wootton SK, Bridle BW, and Karimi K. 2019. Myeloid Cells during Viral Infections and Inflammation. Viruses 11.
30. Elong Ngono A, Vizcarra EA, Tang WW, Sheets N, Joo Y, Kim K, Gorman MJ, Diamond MS, and Shresta S. 2017. Mapping and Role of the CD8(+) T Cell Response During Primary Zika Virus Infection in Mice. Cell Host Microbe 21: 35–46. [PubMed: 28081442]
31. Channappanavar R, Fehr AR, Vijay R, Mack M, Zhao J, Meyerholz DK, and Perlman S. 2016. Dysregulated Type I Interferon and Inflammatory Monocyte-Macrophage Responses Cause Lethal Pneumonia in SARS-CoV-Infected Mice. Cell Host Microbe 19: 181–193. [PubMed: 26867177]
32. Cole SL, Dunning J, Kok WL, Benam KH, Benlahrech A, Repapi E, Martinez FO, Drumright L, Powell TJ, Bennett M, Elderfield R, Thomas C, investigators M, Dong T, McCauley J, Liew FY, Taylor S, Zambon M, Barclay W, Cerundolo V, Openshaw PJ, McMichael AJ, and Ho LP. 2017. M1-like monocytes are a major immunological determinant of severity in previously healthy adults with life-threatening influenza. JCI Insight 2: e91868. [PubMed: 28405622]
33. Michlmayr D, Andrade P, Gonzalez K, Balmaseda A, and Harris E. 2017. CD14(+)CD16(+) monocytes are the main target of Zika virus infection in peripheral blood mononuclear cells in a paediatric study in Nicaragua. Nat Microbiol 2: 1462–1470. [PubMed: 28970482]
34. Foo SS, Chen W, Chan Y, Bowman JW, Chang LC, Choi Y, Yoo JS, Ge J, Cheng G, Bonnin A, Nielsen-Saines K, Brasil P, and Jung JU. 2017. Asian Zika virus strains target CD14(+) blood monocytes and induce M2-skewed immunosuppression during pregnancy. Nat Microbiol 2: 1558–1570. [PubMed: 28827581]
35. Yoshikawa FSY, Pietrobon AJ, Branco A, Pereira NZ, Oliveira L, Machado CM, Duarte A, and Sato MN. 2019. Zika Virus Infects Newborn Monocytes Without Triggering a Substantial Cytokine Response. J Infect Dis 220: 32–40. [PubMed: 30785182]
36. Gorman MJ, Caine EA, Zaitsev K, Begley MC, Weger-Lucarelli J, Uccellini MB, Tripathi S, Morrison J, Yount BL, Dinnon KH 3rd, Ruckert C, Young MC, Zhu Z, Robertson SJ, McNally KL, Ye J, Cao B, Mysorekar IU, Ebel GD, Baric RS, Best SM, Artyomov MN, Garcia-Sastre A, and Diamond MS. 2018. An Immunocompetent Mouse Model of Zika Virus Infection. Cell Host Microbe 23: 672–685 e676. [PubMed: 29746837]
37. Wu KY, Zuo GL, Li XF, Ye Q, Deng YQ, Huang XY, Cao WC, Qin CF, and Luo ZG. 2016. Vertical transmission of Zika virus targeting the radial glial cells affects cortex development of offspring mice. Cell Res 26: 645–654. [PubMed: 27174054]
38. Yockey LJ, Varela L, Rakib T, Khoury-Hanold W, Fink SL, Stutz B, Szigeti-Buck K, Van den Pol A, Lindenbach BD, Horvath TL, and Iwasaki A. 2016. Vaginal Exposure to Zika Virus during Pregnancy Leads to Fetal Brain Infection. Cell 166: 1247–1256 e1244. [PubMed: 27565347]
39. Fernandez E, Dejnirattisai W, Cao B, Scheaffer SM, Supasa P, Wongwiwat W, Esakky P, Drury A, Mongkolsapaya J, Moley KH, Mysorekar IU, Screaton GR, and Diamond MS. 2017. Human antibodies to the dengue virus E-dimer epitope have therapeutic activity against Zika virus infection. Nat Immunol 18: 1261–1269. [PubMed: 28945244]

40. Winkler CW, Woods TA, Rosenke R, Scott DP, Best SM, and Peterson KE. 2017. Sexual and Vertical Transmission of Zika Virus in anti-interferon receptor-treated Rag1-deficient mice. Sci Rep 7: 7176. [PubMed: 28775298]
41. Lazear HM, Govero J, Smith AM, Platt DJ, Fernandez E, Miner JJ, and Diamond MS. 2016. A Mouse Model of Zika Virus Pathogenesis. Cell Host Microbe 19: 720–730. [PubMed: 27066744]
42. Grant A, Ponia SS, Tripathi S, Balasubramaniam V, Miorin L, Sourisseau M, Schwarz MC, Sanchez-Seco MP, Evans MJ, Best SM, and Garcia-Sastre A. 2016. Zika Virus Targets Human STAT2 to Inhibit Type I Interferon Signaling. Cell Host Microbe 19: 882–890. [PubMed: 27212660]
43. Tashiro H, Takahashi K, Hayashi S, Kato G, Kurata K, Kimura S, and Sueoka-Aragane N. 2016. Interleukin-33 from Monocytes Recruited to the Lung Contributes to House Dust Mite-Induced Airway Inflammation in a Mouse Model. PLoS One 11: e0157571. [PubMed: 27310495]
44. Winkler CW, Myers LM, Woods TA, Carmody AB, Taylor KG, and Peterson KE. 2017. Lymphocytes have a role in protection, but not in pathogenesis, during La Crosse Virus infection in mice. J Neuroinflammation 14: 62. [PubMed: 28340587]
45. Winkler CW, Myers LM, Woods TA, Messer RJ, Carmody AB, McNally KL, Scott DP, Hasenkrug KJ, Best SM, and Peterson KE. 2017. Adaptive Immune Responses to Zika Virus Are Important for Controlling Virus Infection and Preventing Infection in Brain and Testes. J Immunol 198: 3526–3535. [PubMed: 28330900]
46. Winkler CW, Race B, Phillips K, and Peterson KE. 2015. Capillaries in the olfactory bulb but not the cortex are highly susceptible to virus-induced vascular leak and promote viral neuroinvasion. Acta Neuropathol 130: 233–245. [PubMed: 25956408]
47. Winkler CW, and Peterson KE. 2018. Using immunocompromised mice to identify mechanisms of Zika virus transmission and pathogenesis. Immunology 153: 443–454. [PubMed: 29266213]
48. Ben Amara A, Gorvel L, Baulan K, Derain-Court J, Buffat C, Verollet C, Textoris J, Ghigo E, Bretelle F, Maridonneau-Parini I, and Mege JL. 2013. Placental macrophages are impaired in chorioamnionitis, an infectious pathology of the placenta. J Immunol 191: 5501–5514. [PubMed: 24163411]
49. Lang J, Cheng Y, Rolfe A, Hammack C, Vera D, Kyle K, Wang J, Meissner TB, Ren Y, Cowan C, and Tang H. 2018. An hPSC-Derived Tissue-Resident Macrophage Model Reveals Differential Responses of Macrophages to ZIKV and DENV Infection. Stem Cell Reports 11: 348–362. [PubMed: 29983385]
50. Li Z, Zhao M, Li T, Zheng J, Liu X, Jiang Y, Zhang H, and Hu X. 2017. Decidual Macrophage Functional Polarization during Abnormal Pregnancy due to Toxoplasma gondii: Role for LILRB4. Front Immunol 8: 1013. [PubMed: 28883820]
51. Aldo PB, Racicot K, Craviero V, Guller S, Romero R, and Mor G. 2014. Trophoblast induces monocyte differentiation into CD14+/CD16+ macrophages. Am J Reprod Immunol 72: 270–284. [PubMed: 24995492]
52. Roszer T 2015. Understanding the Mysterious M2 Macrophage through Activation Markers and Effector Mechanisms. Mediators Inflamm 2015: 816460. [PubMed: 26089604]
53. Haghighi Poodeh S, Salonurmi T, Nagy I, Koivunen P, Vuoristo J, Rasanen J, Sormunen R, Vainio S, and Savolainen MJ. 2012. Alcohol-induced premature permeability in mouse placenta-yolk sac barriers in vivo. Placenta 33: 866–873. [PubMed: 22884851]
54. Zeisberger SM, Odermatt B, Marty C, Zehnder-Fjallman AH, Ballmer-Hofer K, and Schwendener RA. 2006. Clodronate-liposome-mediated depletion of tumour-associated macrophages: a new and highly effective antiangiogenic therapy approach. Br J Cancer 95: 272–281. [PubMed: 16832418]
55. Barreto-Vieira DF, Barth OM, Silva MA, Santos CC, Santos Ada S, Filho FJ, and Filippis AM. 2016. Ultrastructure of Zika virus particles in cell cultures. Mem Inst Oswaldo Cruz 111: 532–534. [PubMed: 27581122]
56. Drescher B, and Bai F. 2013. Neutrophil in viral infections, friend or foe? Virus Res 171: 1–7. [PubMed: 23178588]
57. Galani IE, and Andreakos E. 2015. Neutrophils in viral infections: Current concepts and caveats. J Leukoc Biol 98: 557–564. [PubMed: 26160849]

58. van Rooijen N, Kors N, and Kraal G. 1989. Macrophage subset repopulation in the spleen: differential kinetics after liposome-mediated elimination. J Leukoc Biol 45: 97–104. [PubMed: 2521666]

59. Avila-Perez G, Nogales A, Park JG, Marquez-Jurado S, Iborra FJ, Almazan F, and Martinez-Sobrido L. 2019. A natural polymorphism in Zika virus NS2A protein responsible of virulence in mice. Sci Rep 9: 19968. [PubMed: 31882898]

60. Calvet G, Aguiar RS, Melo ASO, Sampaio SA, de Filippis I, Fabri A, Araujo ESM, de Sequeira PC, de Mendonca MCL, de Oliveira L, Tschoeke DA, Schrago CG, Thompson FL, Brasil P, Dos Santos FB, Nogueira RMR, Tanuri A, and de Filippis AMB. 2016. Detection and sequencing of Zika virus from amniotic fluid of fetuses with microcephaly in Brazil: a case study. Lancet Infect Dis 16: 653–660. [PubMed: 26897108]

Key Points

1. Maternal myeloid cells are recruited to the placenta during ZIKV infection.
2. Maternal but not fetal myeloid cells inhibit vertical transmission of ZIKV.
3. Myeloid cells do not contribute to maintenance of the placental barrier.

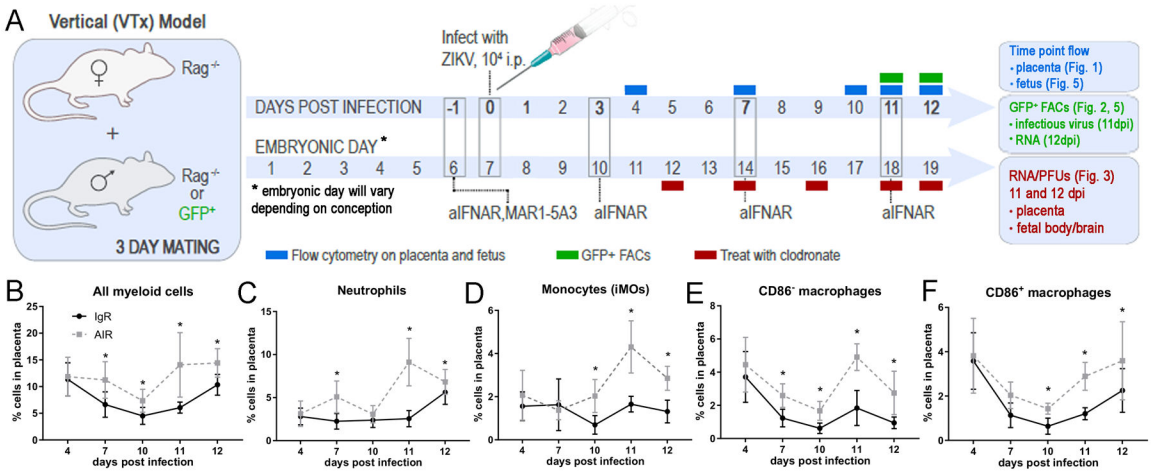

Fig. 1. Myeloid cell infiltration into placenta in ZIKV infected IgR and AIR mice.

(A) Timeline schematic of experimental manipulations for the generation of ZIKV infected, pregnant AIR mice and tissue time point collections. Flow cytometry phenotyping experiments time points are shown in blue. FACs sorting experiment time points for infectious center assays and RNA experiments are shown in green. The injection schedule for myeloid cell depletions are shown in red and the dpi and what tissues were taken. (B-F) Placental tissue was collected from IgR and AIR litters at the indicated timepoints and analyzed via flow cytometry for markers of myeloid cell populations. Plots of all myeloid cells (B), neutrophils (C), monocytes (iMOs) (D), $CD86^{-}$ macrophages (E) and $CD86^{+}$ macrophages (N) populations as a percent of the all placenta cells from IgR (black symbols) and AIR (gray symbols) placentas are shown for each time point during infection. Each dot represents a total of 11–36 placentas for two to four litters from infected IgR or AIR dams (animal number breakdown in materials and methods). Statistical significance was determined using a two-way ANOVA with a Sidak's multiple comparisons test. *=p<0.05, **=p<0.01. Error bars represent standard deviation.

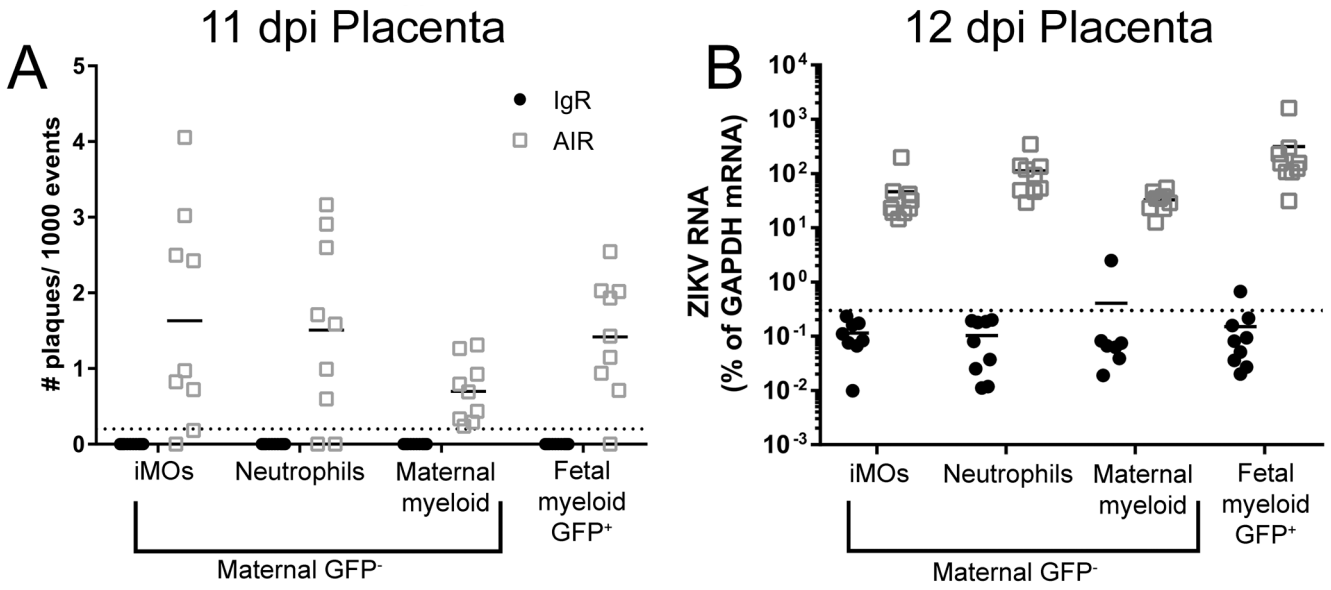

Fig. 2. Maternal and fetal myeloid cells in the placenta contain ZIKV RNA and infectious virus.

Placental immune cell enriched suspensions from 11 and 12dpi IgR and AIR GFP$^+$ heterozygous litters were FACs sorted (Sup. Fig. 2) for myeloid cell populations. Infectious centers at 11dpi (A) or ZIKV RNA at 12dpi (B) for each sorted population from IgR (black symbols) or AIR (gray symbols) placentas was analyzed. Each dot represents sorted cells from a single placenta. Infectious centers are plotted as the number of plaques per 1000 events (cells) plated. Viral RNA was plotted as the percentage of gene expression relative to that of the *Gapdh (*glyceraldehyde 3-phosphate dehydrogenase) gene. The viral RNA level in each sample was calculated as the difference in the percentage in cycle threshold (C_t): C_t for *Gapdh* mRNA minus C_t for viral mRNA. The level of detection for the assay is indicated by the dotted line.

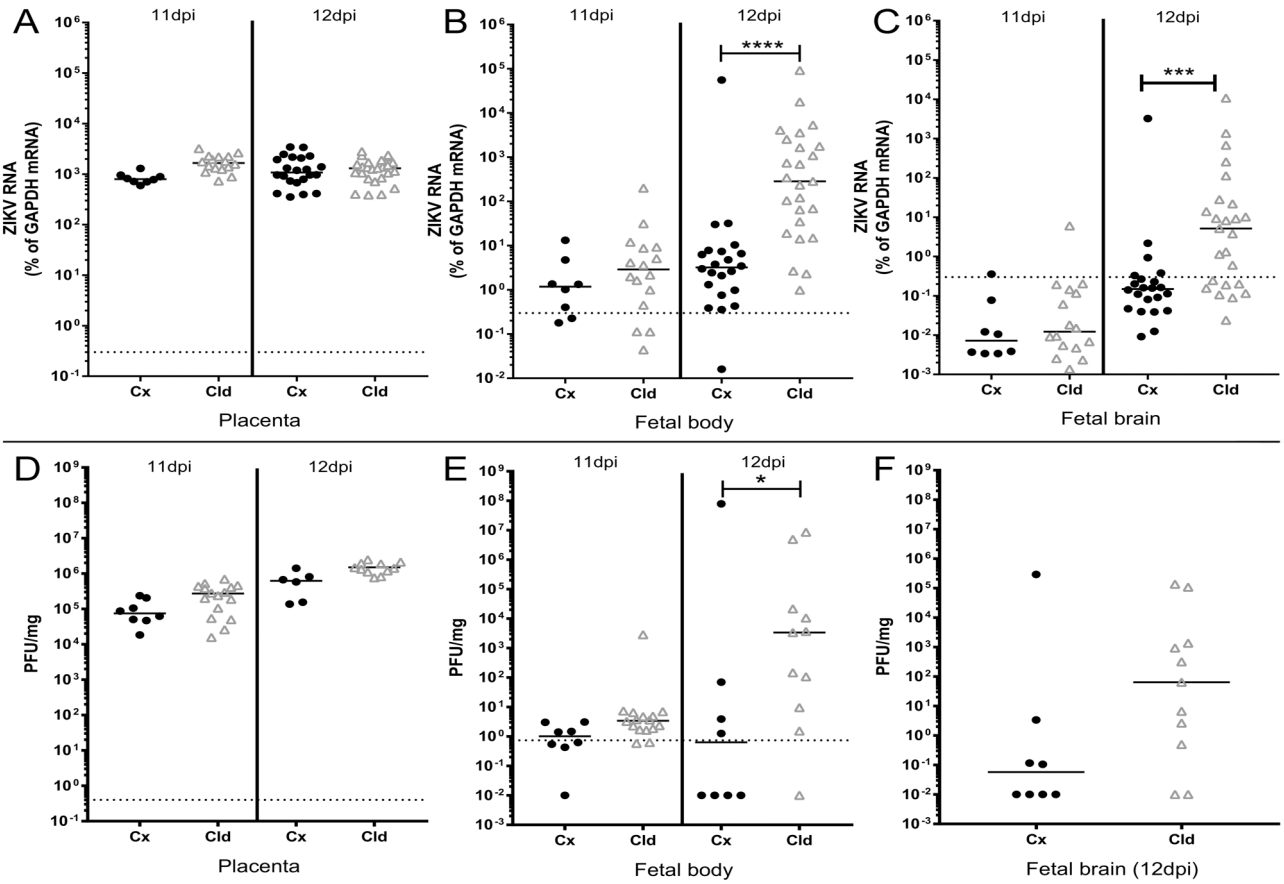

Fig. 3. Depletion of myeloid cells accelerates VTx of ZIKV.

Placental, fetal body and fetal brain tissues were collected from pregnant, infected AIR mice treated with either control (Cx, black symbols) or clodronate (Cld, gray symbols) liposomes at 11 or 12dpi as indicated. Tissues were processed for RNA (A-C) or plaque analysis (D-F) as described in the materials and methods. ZIKV RNA from placenta (A), fetal body (B) and fetal brain (C) was analyzed and plotted as described above (Fig. 2). A Kruskal-Wallis test with a Dunn's multiple comparisons test was used to determine statistical significance. ***=$p<0.001$, ****=$p<0.0001$. Plaque assay data from placenta (D), fetal body (E) and fetal brain (F, 12dpi only) are plotted as plaque forming units per mg of tissue. To determine statistical significance, a Kruskal-Wallis test with a Dunn's multiple comparisons test was run for placenta (F) and fetal body samples (E) and A Mann-Whitney U-test was run for 12dpi fetal brain. *=$p<0.05$.

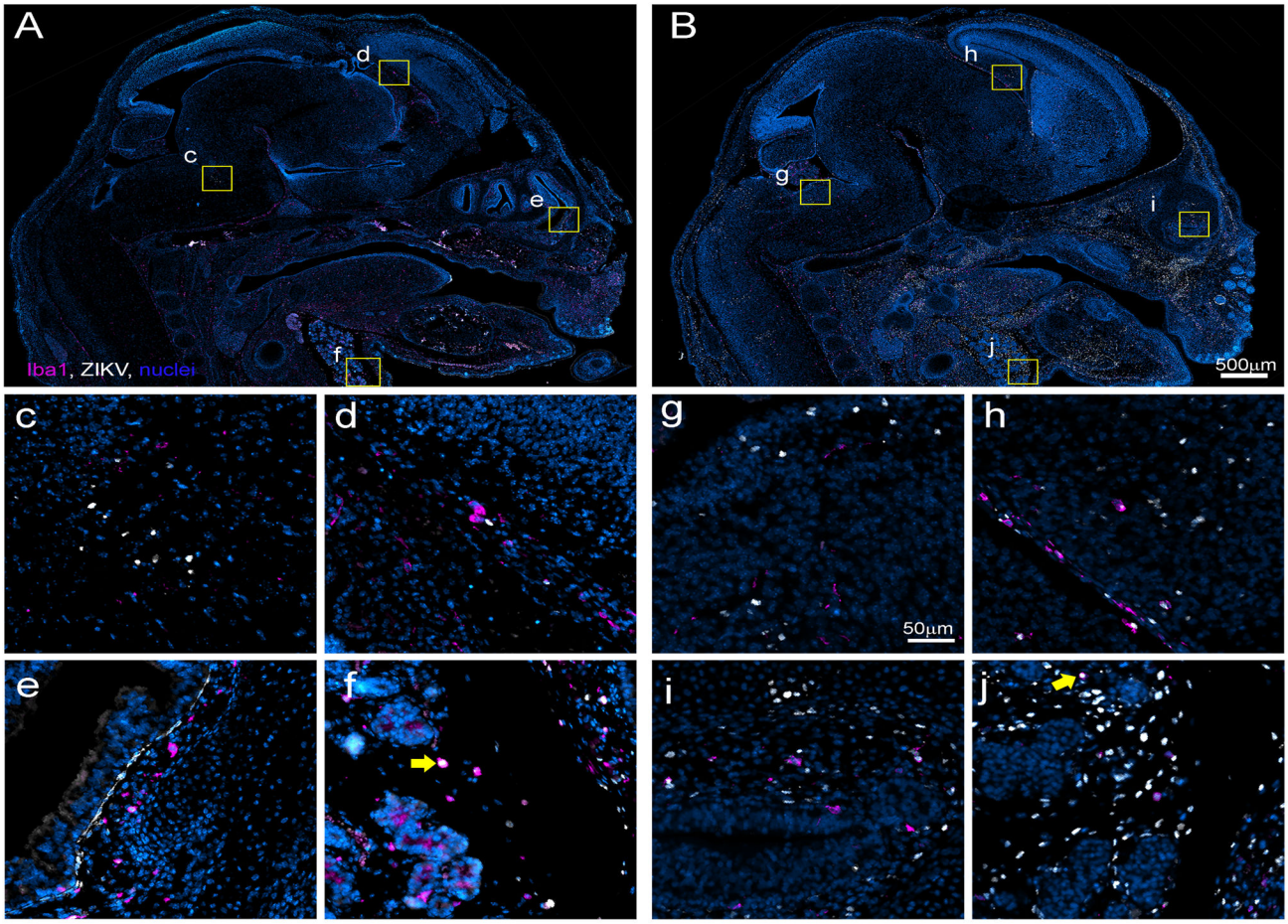

Fig. 4. ZIKV infection is more prevalent and wide spread throughout clodronate treated fetuses.

Fetuses from control (A, c, d, e, f and K) or clodronate (B, g, h, i, j and L) treated litters were immunohistologically labeled for ZIKV NS5 protein (white) indicating infection and Iba1 (magenta) indicating myeloid lineage cells. Representative 40x composite images demonstrate the extent of ZIKV infection and myeloid distribution within the head and neck region of fetuses from control (A) and clodronate (B) treated litters. Zoomed insets from the brain (control c, d and clodronate g, h), olfactory epithelium (control e and clodronate i) and submaxillary salivary gland region (control f and clodronate j) of fetuses demonstrate representative ZIKV infection and associated myeloid cells. The yellow arrows in (f and j) indicate $Iba1^{+}$ myeloid cells that are also positive for ZIKV NS5.

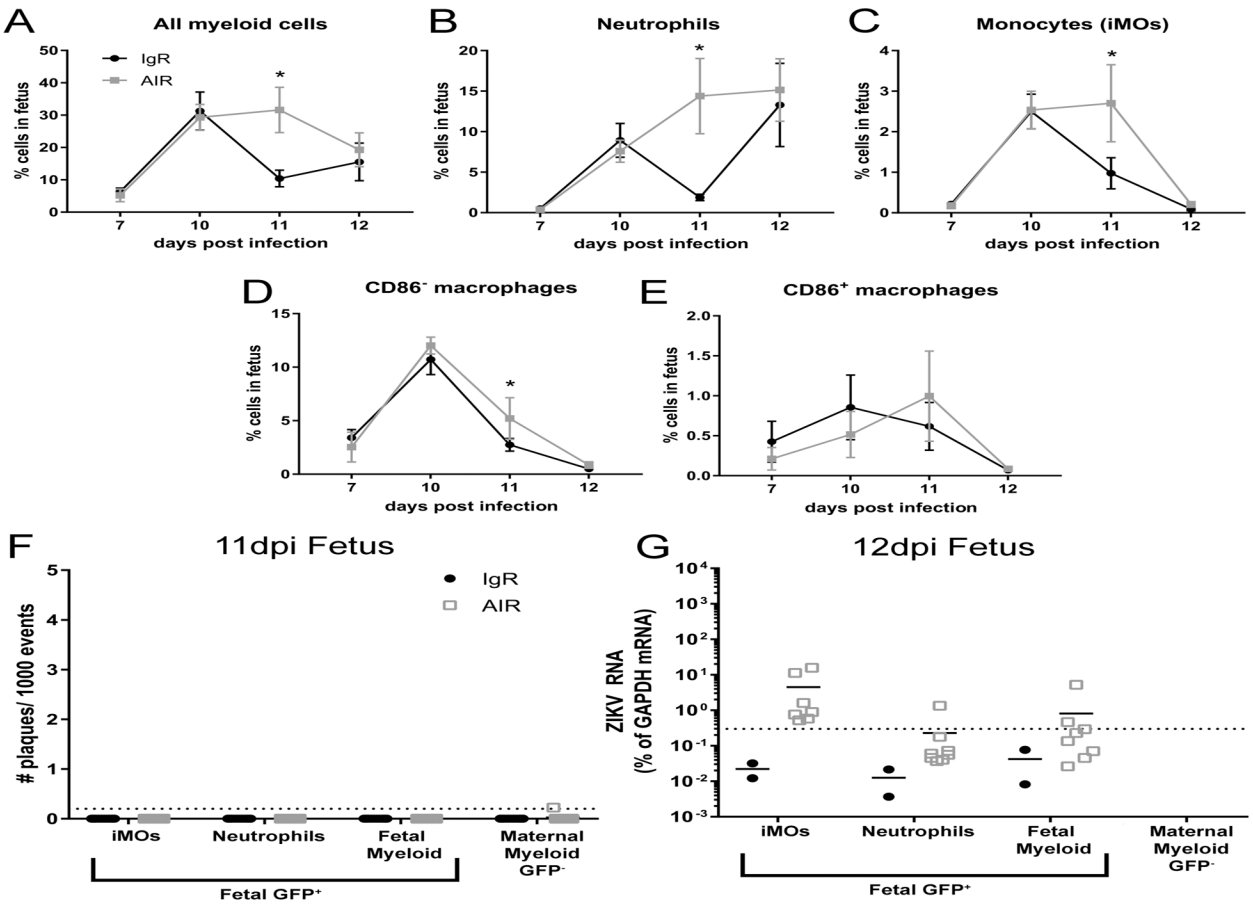

Fig. 5. Myeloid cells in the fetus are insufficient to protect against ZIKV infection.

From some of the same litters at the 7–12dpi time points shown in Fig. 1, myeloid cells populations isolated from the whole fetus were analyzed using the same flow cytometry gating strategy (Sup. Fig. 1). Plots of all fetal myeloid cells (A), neutrophils (B) and monocytes (iMOs, C), $CD86^{-}$ macrophages (D) and $CD86^{+}$ macrophages (E) are shown as a percent of that cell population within the whole fetus. A two-way ANOVA with a Sidak's multiple comparisons test was performed to determine statistical significance. *=$p<0.05$. Error bars represent standard deviation. From the same 11 and 12dpi IgR or AIR GFP^{+} heterozygous litters shown in Fig. 2, Percoll enrich myeloid cells were isolated and sorted from the whole fetus and analyzed for infectious centers (F) or ZIKV RNA (E) expression using the same strategy. At 12dpi, too few maternal myeloid cells were obtained from either treatment group for RNA analysis to be performed.

Table 1:

Virus infection in fetus from clodronate and control-liposomes treated dams.

Tissue Region[a]	Control liposome	Clodronate liposome
Whole fetus	5/13 (38.5 %)	21/26 (80.8%)
Lymph node	2/13 (15.4%)	13/26 (50.0%)
Nasal turbinates	3/13 (23.1%)	15/26 (57.7%)
Choroid plexus	1/13 (7.7%)	8/26 (30.8%)
Meningies	2/13 (15.4%)	10/26 (38.5%)
Head neck	5/13 (38.5%)	14/26 (53.8%)
Brain	1/11 (9.1%)	12/23 (52.2%)
Spinal cord	0/11	5/23 (26.1%)
Muscle	0/13	4/26 (15.4%)
Plural organs[b]	0/13	4/26 (15.4%)
Abdominal organs[c]	0/13	5/26 (15.4%)

[a] all determinations of tissue infection were determined by anatomical reference { http://www.emouseatlas.org } and did not involve immunohistochemical phenotyping except for lymphatics which were determined by Iba1+ labeling

[b] indicates if ZIKV antigen was observed in any organ within the plural cavity

[c] indicates if ZIKV antigen was observed in any organ within the abdominal cavity